Progress In Electromagnetics Research B, Vol. 98, 1–19, 2023

Gain-bandwidth Enhancement of Tapered Fed Ellipsoid Antenna for EWB (23.16–776.59 GHz) Applications Using EBG

Naineri Suguna and Senthil Revathi*

Abstract—A compact extreme wide band (EWB) modified ellipsoid monopole antenna utilising electromagnetic band gap (EBG) technology is developed on a Rogers RT/Duroid 5880 substrate for high frequency millimetre (mm) wave applications including cellular, satellite, radar, and medical imaging. The proposed antenna design has an overall dimension of 40 mm × 30 mm × 0.787 mm and achieves EWB characteristics with a frequency range of 23.16 GHz to 776.59 GHz, a fractional impedance bandwidth (FBW) of 188.41%, and a bandwidth ratio (BR) of 33.53 by using a tapered feed and an EBG technique. The proposed antenna design attained a maximum peak gain of 17.91 dB and a peak radiation efficiency of 99.4%. On the basis of its high impedance wide bandwidth (IBW), FBW, BR, peak gain, and peak radiation efficiency, as well as its omnidirectional radiation properties at resonant frequencies, this compact antenna has the potential to be utilised for EWB applications. The HFSS 3-D solver is applied to characterize and analyse antenna performance.

1. INTRODUCTION

With advances in wireless communication, there has been a significant increase in cellular applications such as mobile phones, routers, iPads, and laptops. Communication systems have advanced dramatically in recent years. In this wireless world, there are various generations determined by the increased number of cellular networks. The parameters for modern technology should take into account factors such as small size, wider bandwidth, and cost-effectiveness. Ultra-Wide Band (UWB) technology is becoming more popular in wireless personal area networks. For wireless applications, the UWB frequency ranges from 3.1 to 10.6 GHz. People seek to employ Super Wide Band (SWB) applications because mobile connectivity is congested and has various limitations. SWB has the capacity to transmit data over both short and long distances. The specifications of super wideband provide a large channel capacity, high resolution, and 10 : 1 or more bandwidth ratio (BR). This means that the frequency is higher, and the timing precision is higher. In view of technological advancements, super wideband is one approach for making the system faster and more accurate.

In article [1], a compact microstrip patch antenna with a 24 mm × 18 mm × 0.787 mm size is proposed using an RT Duroid substrate and a club-like patch to attain super-wideband properties. It operates at frequencies ranging from 50 to 200 GHz. However, the gain parameter has a limitation. Ref. [2] proposes a microstrip-fed, planar monopole antenna with three frequency bands. For WLAN, WiMAX, and X-band applications, the proposed antennas have frequencies ranging from 3.34–4.8 GHz, 5.5–10.6 GHz, and 13–14.96 GHz, but achieve a narrow bandwidth. In paper [3], a semicircular monopole antenna with a super wideband patch that has a high impedance bandwidth ratio of 15.38 : 1 and BDR of 4261.007 is presented. The dimensions of the antenna are 52.25mm × 42 mm × 1.57 mm. In the work [4], an ultra-wideband planar monopole antenna with a reduced ground plane of $11 \times 15\,\text{mm}^2$ on an FR4 substrate is proposed. The frequency range is 5–15 GHz, and the VSWR is less than 2.5. However, the

Received 11 October 2022, Accepted 5 December 2022, Scheduled 15 December 2022
* Corresponding author: Senthil Revathi (srevathi@vit.ac.in).
The authors are with the School of Electronics Engineering, Vellore Institute of Technology, Vellore 632014, India.

bandwidth and gain constitute a problem. The proposed antenna design contains a U-slot on the patch, a triangle slot, and two flipped U-slots on the ground. It has a size of $25 \times 26\,\text{mm}^2$, a frequency range of 2.43–32.93 GHz, and an acceptable gain of 2.73 dBi to 7.35 dBi. Work [6] evaluates an inverted-core, low-profile antenna with a UWB slot. The antenna is 40 mm × 40 mm in size, with a bandwidth of 3 GHz to 18 GHz and a maximum gain of 3.2 dB. A concept for a small hexagonal Sierpinski fractal antenna that can be used for super wideband applications is proposed in paper [7]. The bandwidth ranges from 3.4 to 37.4 GHz. In paper [8], a miniature UWB antenna with a low profile is presented with a technique for the enhancement of bandwidth and stability in the radiation pattern. The antenna is about $30 \times 10\,\text{mm}^2$ and has a range of frequencies from 3.1 GHz to 10.6 GHz. Design [9] presents a coplanar waveguide (CPW) transparent antenna with UWB applications for bandwidth enhancement with dimensions of $30 \times 45 \times 0.175\,\text{mm}^3$ and frequency ranges of 3.15 to 32 GHz, but the limitation is that the size of the antenna is large, but the gain and bandwidth are small. In paper [10], a 14 mm × 22 mm × 1.6 mm monopole antenna is proposed for the use in ground-penetrating radar. The frequency ranges from 3.9 to 18 GHz, but it has lower radiation efficiency characteristics. In paper [11], a propeller-shaped monopole patch antenna with a CPW feed is given for super wideband applications. Its frequency range is between 3 and 35 GHz, and its gain varies between 4 and 5.2 dBi. In paper [12], a $20 \times 28\,\text{mm}^2$ cactus-shaped monopole antenna for ultra-broadband applications is described. The frequency ranges from 2.85 to 11.85 GHz. Bandwidth is about 9 GHz, and gain is 3.2 dBi. A small monopole antenna with a phi-shaped pattern is described in this design [13] for super-wideband operations. The bandwidth of impedance varies from 3.5 to 37.2 GHz. Efficiency varies between 3.9 and 18 GHz; however, radiation efficiency characteristics are lower. In design [14], a UWB coplanar strip with a CPW-fed rectangular spiral antenna is described. The antenna size is about $50 \times 40 \times 0.508\,\text{mm}^3$, with a frequency range of 3.5–10.6 GHz and peak gain range of 1–4.7 dBi. In this design, a miniature microstrip patch antenna in the shape of a crescent is proposed for the use in super wideband applications [15]. It has a size of $32 \times 22\,\text{mm}^2$ and frequency range of 2.5 to 29 GHz. For UWB applications, paper [16] proposes a miniature printed planar monopole radiator. The antenna has dimensions of around $35 \times 30 \times 1.52\,\text{mm}^3$ with a bandwidth of 10.1 GHz. The time domain and frequency domain performance of a printed super wideband antenna is presented in this design [17], with a VSWR less than two and frequency ranges ranging from 400 MHz to 16 GHz. In design [18], a compact wideband antenna with an L-shaped radiating element size of $30 \times 30 \times 1.6\,\text{mm}^3$ and an F4B substrate material with 1.6 mm height are utilised. The operating frequency of an antenna ranges from 2.11 to 5.01 GHz. A printed wideband antenna with a trapezoidal ground and an elliptical monopole antenna is described in [19]. The antenna is 110 mm × 124 mm in size and has frequency ranges of 1.05–224.1 GHz. In [20], a CPW and microstrip line UWB antenna in the shape of a scarecrow is described. The antenna is 110 mm × 124 mm in size, with frequency ranges from 1.05 to 224.1 GHz. An elliptical monopole and trapezoid ground with a printed super-wideband is depicted in design [21]. The antenna is about 120 mm × 124 mm in size, and its frequency varies from 1.08 to 27.4 GHz. Multiband monopole antennas with an O-shape and different patch orientations are implemented in paper [22] for various UWB and wireless LAN applications. The size of the designed antenna is about $60 \times 50\,\text{mm}^2$. The developed design does not meet the results criteria, which is the limitation. Two printed planar monopole antennas are presented in paper [23], with dimensions of 47.85 mm × 35 mm and a thickness of 1.524 mm. [24] describes a CPW-fed SWB. The antenna size is $140 \times 100\,\text{mm}^2$; the frequency spans from 400 MHz to 20 GHz; and the gain is 6.3 dBi. A super compact parasitic patch antenna and a gain enhancement for super wideband applications are described in [25]. The antenna is $12 \times 4.6 \times 0.8\,\text{mm}^3$ in size with a bandwidth of 16 GHz. This design [26] employs a printed monopole antenna with CPW feed for ultra-high UWB applications. The frequency range is between 4.9 and 25 GHz, and the typical gain is 4 dBi. In study [27], an SWB microstrip fractal antenna for 5G communication is presented employing a star-shaped fractal geometry to generate a snowflake-like structure. The antenna is 20 mm × 20 mm in size, and its operating frequency extends from 17.22 GHz to 180 GHz. A circular monopole with a partially segmented elliptical slot for SWP applications is presented in work [28]. Its frequency varies around 0.96 GHz and 10.9 GHz, and its VSWR is less than 2. However, while the antenna is tiny, it has a low bandwidth ratio of 11.01:1. In paper [29], a miniature SWB antenna for mobile applications is proposed. A rectangular notch and a ground plane with semi-circular notches are used to increase the impedance bandwidth. The bandwidth of impedance is 3–60 GHz. In work [30], CSRR, SRR, and DGS are combined to provide a penta-notched

UWB antenna with sharp frequency edge selectivity. Due to its small size, it can be used for portable communication. By maintaining a miniaturised structure, these wideband, UWB, and SWB antennas failed to provide wide impedance bandwidth, maximum peak, and radiation efficiency. The challenge is to keep the antenna low-profile and miniature even while improving all of these criteria.

The literature motivates the authors to design one novel miniaturised antenna to enhance all the necessary parameters by maintaining various suitable applications. In this work, a tiny tapered-fed modified ellipsoid patch radiator using electromagnetic band gap (EBG) methodology is proposed for wireless applications such as cellular applications, radar systems, satellite communications, mm-wave applications, and medical imaging applications. The proposed antenna exhibits an extreme wide bandwidth (EWB) of 753.43 GHz within the operating spectrum from 23.16 GHz to 776.59 GHz, having a maximum reflection coefficient of −37.21 dB. Within the operating band, the design also has a peak gain of 17.91 dB and a radiation efficiency of 99.4%.

2. PROPOSED DESIGN GEOMETRY, CONFIGURATION AND RESULTS DISCUSSION

Figure 1 illustrates the final configuration of the proposed extreme wide band (EWB) antenna with an energy band gap (EBG) structure. The suggested structure is developed by Ansys computational electromagnetic (EM) high-frequency structure simulator (HFSS) tool and printed on Rogers RT/Duroid 5880 TM dielectric substrate material, which has the following properties: relative permittivity $(\varepsilon_r) = 2.2$, dissipation factor $(\tan\delta) = 0.0009$, and thickness $(H) = 0.787$ mm. The suggested antenna is developed using four iterations of a conventional microstrip patch antenna (MPA). The following subsections describe a detailed investigation into the implementation of the proposed antenna.

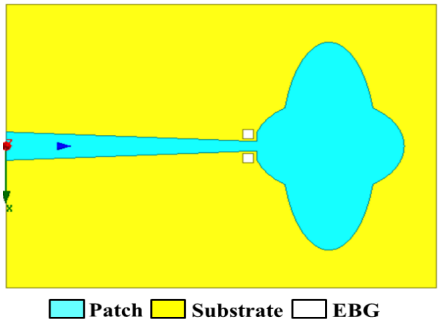

Figure 1. Suggested concentric EWB patch antenna with EBG structure.

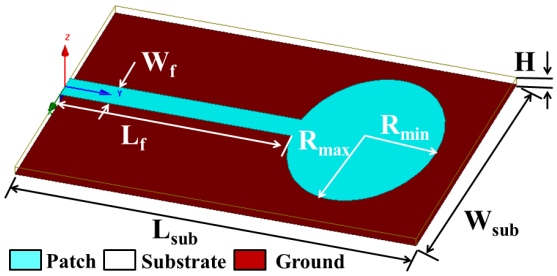

Figure 2. Geometry of conventional elliptical monopole antenna with full ground.

2.1. Conventional Elliptical Monopole Antenna (CEMA)

A transmission line feed, typical elliptical-shaped patch is initially printed on top of the substrate, and a full ground plane is printed on the bottom side. The feeding system has a 50 Ω microstrip line for impedance matching. The geometrical dimensions of conventional antenna designs are measured using standard mathematical calculations [31, 32]. Wide band (WB) has been directly designed from a conventional ellipse structure with optimised dimensions of the radiating patch and feed line to enhance impedance bandwidth (IBW) and other performance characteristics. Table 1 shows the optimised geometrical dimensions of a conventional antenna. The conventional elliptical monopole patch antenna with a 50 Ω transmission line fed at full ground is illustrated in Figure 2. The feed line is 23 mm in length and 3 mm in width.

The reflection coefficient (S_{11}) characteristics of a conventional elliptical-shaped monopole antenna developed using Rogers RT/Duroid 5880 dielectric substrate material are shown in Figure 3. This antenna achieves wide band characteristics in the desired spectrum, though some notch bands are obtained. There are five multiple bands in the intended reflection coefficient characteristics.

Table 1. Geometrical aspects of proposed EWB antenna (All units-mm).

L_{sub}	W_{sub}	L_f	W_f	$R_{\max}$	$R_{\min}$	H
40	30	23	3	11	7	0.787
R_1	R_2	R_3	R_4	W_1	W_2	S_1
11	4.4	7	5	3	1	1

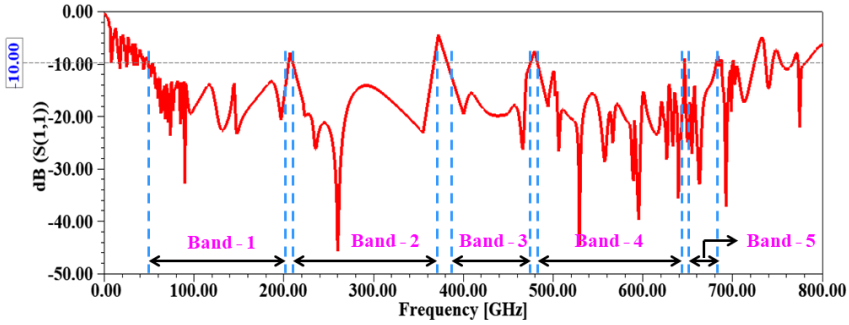

Figure 3. Reflection coefficient characteristics of monopole antenna with full ground.

Impedance bandwidths (IBW) are 152.67 GHz, 156.59 GHz, 91.82 GHz, 163.37 GHz, and 34.93 GHz, respectively, over operating bandwidths of 53.63–205.30 GHz, 210.36–366.95 GHz, 382.29–474.11 GHz, 482.48–645.85 GHz, and 646.13–681.06 GHz. The bandwidth ratio (BR) for band-1 is 3.828, for band-2 is 1.744, for band-3 is 1.24, for band-4 is 1.338, and for band-5 is 1.054. Hence, the main goal of this investigation is to achieve super wide-band characteristics. This conventional structure has been modified to avoid these notch resonances, and its electrical properties are discussed in the following subsection.

2.2. Modified Ellipsoid Monopole Antenna (MEMA)

The conventional elliptical structure can be modified into a novel plus-shaped ellipsoid model to improve impedance bandwidth and avoid notch bands. This new model improves overall impedance in the desired spectrum. Figure 4 shows the modified novel radiating element of the proposed antenna configuration. The optimised dimensions of the designed monopole antenna are listed in Table 1. The S_{11} characteristics of the proposed antenna, which result in wide band return loss characteristics, are represented in Figure 5. The designed antenna has tri-band electrical characteristics. Band-1 operates at frequencies ranging from 35.32 GHz to 206.65 GHz with an impedance bandwidth of 171.33 GHz and a maximum reflection coefficient of −28.17 dB. The IBW of band-2 is 282.42 GHz, with a frequency range of 231.64 to 514.06 GHz. At 321 GHz, its bandwidth ratio is 2.219, and its maximum reflection coefficient is −35 dB. Band-3 operates between 516.09 GHz and 758.50 GHz with a reflection

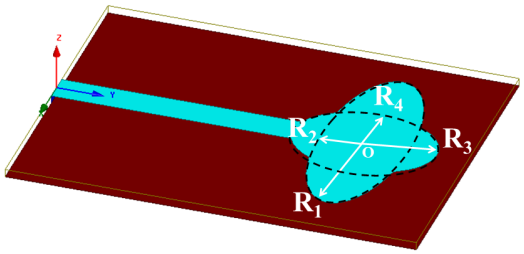

Figure 4. Modified ellipsoid monopole antenna configuration.

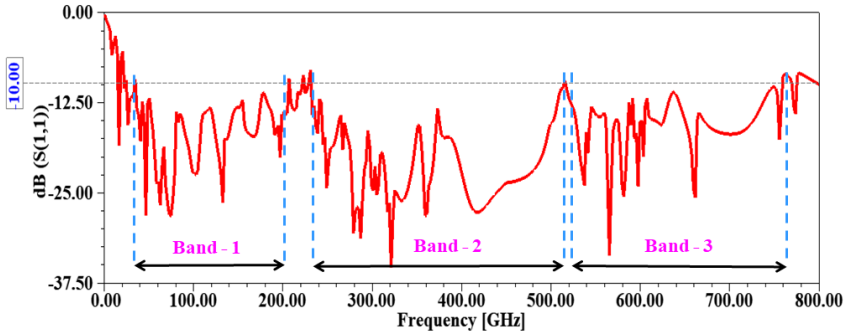

Figure 5. Impedance bandwidth response of modified ellipsoid antenna.

coefficient of −33.55 dB at 564 GHz, and the corresponding impedance bandwidth and bandwidth ratio are 242.41 GHz and 1.46. This design includes two notch bands ranging from 206.65 to 231.64 GHz and 514.06 to 516.09 GHz. It does not meet the design requirements.

2.3. Tapered fed Modified Ellipsoid Monopole Antenna (TMEMA)

Figure 6 shows the tapered geometrical structure of a modified ellipsoid antenna fed with a transmission line. The optimised maximum and minimum widths of the tapered feed line are $W_1 = 3$ mm and $W_2 = 1$ mm. Reflection coefficient (S_{11}) characteristics of the designed antenna are represented in Figure 7. The tapered structure has numerous advantages, such as wide bandwidth, high radiation efficiency, low weight, easy fabrication, planar structure, good directional radiation characteristics, and easy compatibility with microwave integrated circuits (MICs). This tapered structure has a super wide band (SWB) from 39.02 GHz to 713.85 GHz. Compared to previous designed structures [1–30], the

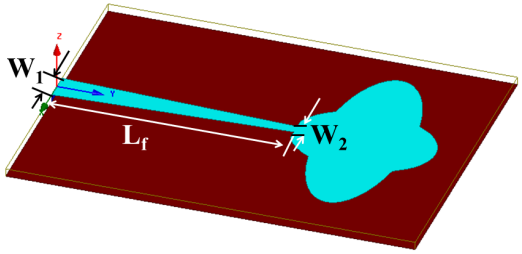

Figure 6. Geometrical configuration of Tapered fed ellipsoid antenna design.

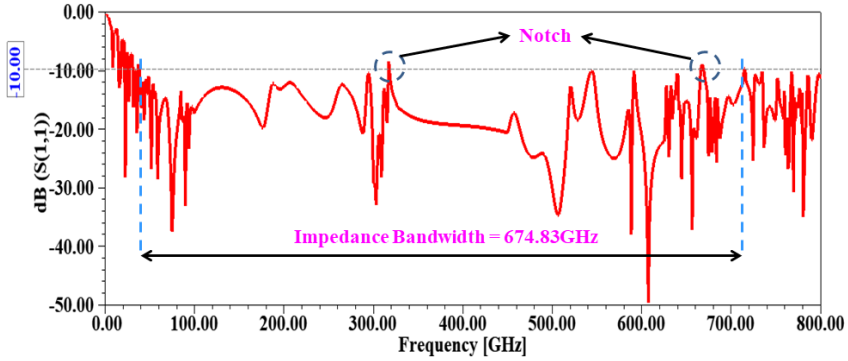

Figure 7. Impedance bandwidth response of designed tapered fed modified ellipsoid configuration.

impedance bandwidth obtained for this designed structure is very large, at 674.83 GHz. With this advantage, the proposed antenna is well suited for advanced wireless, cellular, radar systems, satellites, and limited Terahertz (THz) spectrum applications. Within the operational bandwidth, there are two notch bands at 316.80–317.87 GHz and 665.6–66.83 GHz. These notches caused interference with the stated applications.

2.4. Proposed Tapered Fed Modified Ellipsoid Monopole Antenna with EBG Structure (TMAEBG)

To overcome the notch limitations mentioned above, electromagnetic band gap (EBG) technology, as shown in Figure 6, is incorporated into the designed antenna. The proposed geometrical configuration of the designed antenna is represented in Figure 8. Optimized EBG slots in the design reflect small electromagnetic (EM) waves. The ability of these EBGs to discriminate EM waves can be improved by incorporating slots into the substrate. It creates high densities. These features make the proposed antenna suitable for the use as an EM radiation sensor.

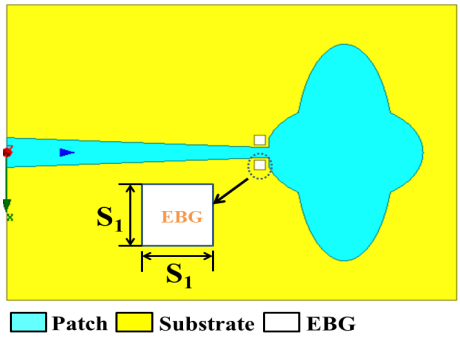

Figure 8. Proposed electromagnetic band gap (EBG) configurations for a tapered fed monopole antenna.

Figures 9(a)–(d) depict the electrical parameters of the proposed antenna, including the input impedance (Zin), group delay (td), reflection coefficient (S_{11}), and voltage standing wave ratio (VSWR). The suggested antenna's S_{11} properties are represented in Figure 9(a). The proposed structure resonates from 23.16 GHz to 776.59 GHz. This frequency band is suitable for millimetre (mm) wave applications, as it covers the extremely high frequencies (EHFs) of 30–300 GHz, as defined by the IEEE Microwave Bands. The proposed antenna resonates not only in the extremely high frequency (EHF) range, but also to a limited extent in the infrared region (300 GHz–400 GHz) up to 776.59 GHz. The proposed antenna has a bandwidth ratio of 33.53 and an impedance bandwidth of 753.43 GHz. Fractional bandwidth (FBW), which is a measure of bandwidth based on wideband characteristics, is 188.41%, which can be written as $FBW = \frac{2*(f_h - f_l)}{(f_h + f_l)} * 100$, where f_l and f_h are lower and higher frequencies at $S_{11} \leq -10$ dB. Figure 9(b) shows the VSWR plot of the proposed antenna, which was simulated using the HFSS tool. This graph demonstrates the impedance-matching condition in terms of VSWR versus frequency. Ideal VSWR values vary between 0 and infinity. In practice, VSWR is lower than two. The VSWR of the proposed antenna is less than two across the entire frequency range for which it is reliable. Group delay (td) is another factor that has been analysed to validate the proposed SWB system. Group delay refers to the degree of the average time lag of a given input in the operating bandwidth. The group delay value of designed antennas is less than or equal to 1 ns at resonance frequency. These group delay characteristics determine the level of distortion in the received signal. The group delay response of the proposed tapered modified ellipsoid structure with an EBG structure is shown in Figure 9(c). The group delay value in the operational region is less than 200 ps (or 0.2 ns). These characteristics maintain linear phase across the operating frequency range. Group delay has a high anticipatory potential against pulse dispersion. Group delay shows good anticipatory potential against pulse dispersion. Figure 9(d)

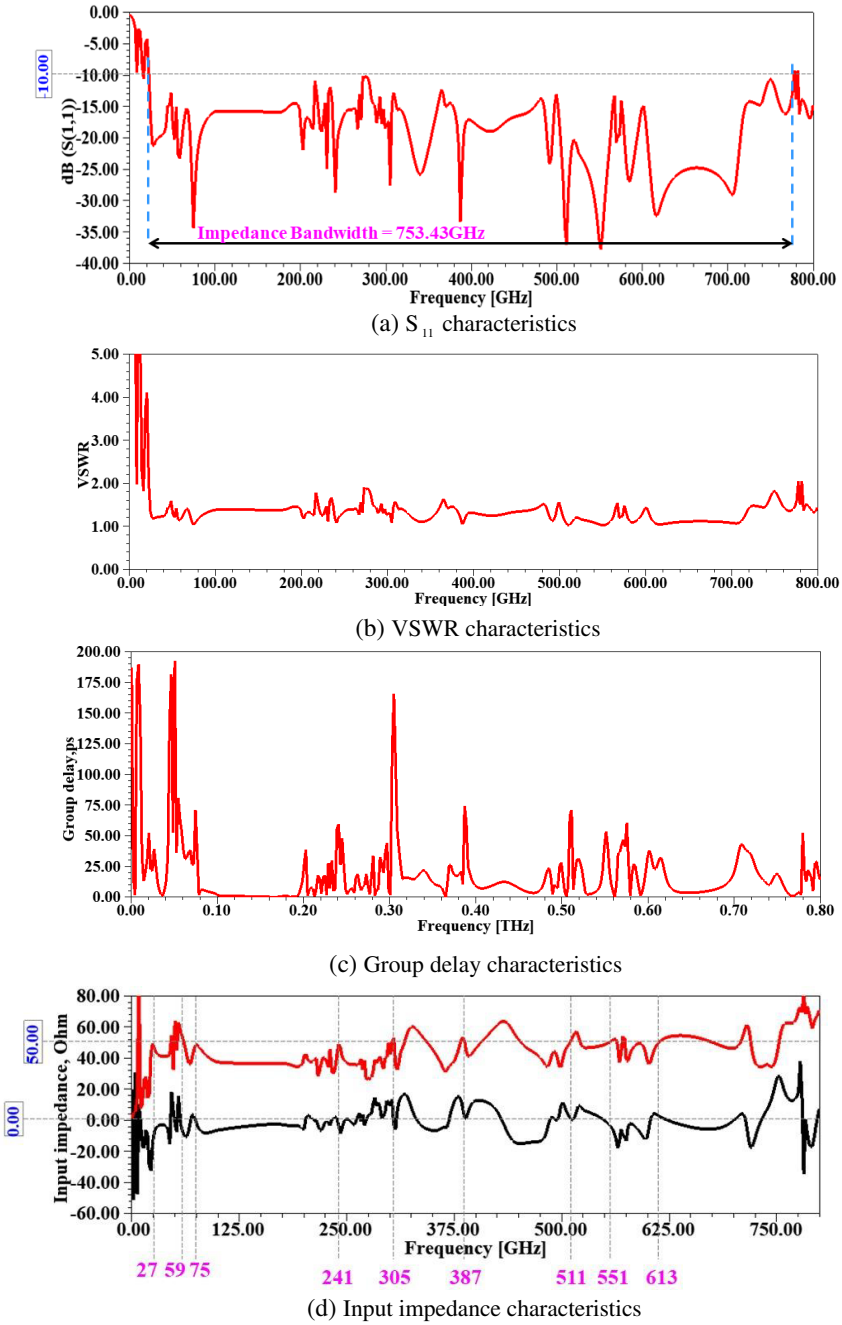

Figure 9. Electrical characteristics of proposed antenna with EBG structures.

shows the input impedance characteristics of the proposed antenna and depicts seven resonant modes at frequencies where the reflection coefficient is maximized. When resonances occur, the reactive and resistive components of the impedance approach 0 and 50, respectively. This indicates that the impedances are properly matched. Table 2 shows the resistive and reactive impedance values of the proposed antenna at the resonance frequencies shown in Figure 9(d).

2.5. EBG Design and Analysis

In this EBG technique, a portion of the substrate beneath the antenna's radiating patch is removed, resulting in a low effective dielectric constant. As a result, power loss due to surface wave excitation is

Table 2. Values of resistive and reactive input impedances at resonances.

Resonant mode	Frequency, GHz	Resistive input impedance	Reactive input impedance
1	27	45.88 Ω	−7.42 Ω
2	59	54.37 Ω	−5.65 Ω
3	75	48.17 Ω	−0.43 Ω
4	241	48.68 Ω	−3.35 Ω
5	305	53.05 Ω	−3.05 Ω
6	387	50.97 Ω	1.95 Ω
7	511	51.32 Ω	0.59 Ω
8	551	50.67 Ω	−4.03 Ω
9	613	50.18 Ω	2.77 Ω

reduced, and power coupling to space waves is improved. EBG structure behaves as a high-impedance surface when being implemented as an LC network. These EBG cells also have a stopband that prevents the propagation of surface waves. The properties of EBG are used in the substrate design of the proposed antenna to achieve its extreme bandwidth characteristics.

The parameters represented in the EBG geometry are substrate thickness h, width of the patch element $W(= S_1)$, gap between patches g, dielectric constant ε_r, and EBG slab dimensions $(S_1 \times S_1)$. When the periodicity $(W + g)$ is small compared to the operating wavelength, the operation mechanism of this EBG structure can be explained using an effective medium model with equivalent lumped LC elements [33], as shown in Figure 10.

The impedance of the parallel LC-circuit is given by

$$Z = \frac{j\omega L}{1 - \omega^2 LC}, \text{ where resonant frequency } \omega = 1/\sqrt{LC}. \tag{1}$$

The inductor L and capacitor C values for an EBG structure with patch and gap width, substrate thickness (h), dielectric constant (ε_r), and vias radius (r) are calculated using the formula below [35, 36], and their geometries are shown in Figure 10 and Figure 11.

$$L = \mu_0 h \tag{2}$$

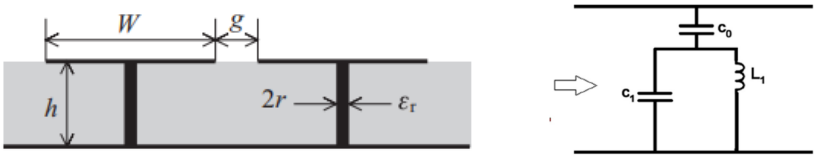

Figure 10. Geometries of (a) Parameters for the structure of mushroom-like EBG, (b) Lumped LC model.

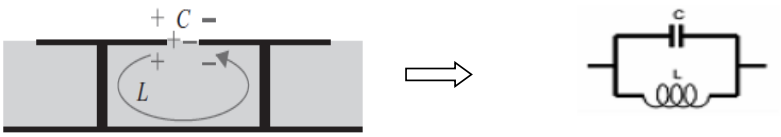

Figure 11. Typical Lumped LC model of EBG structure.

$$C = \frac{W\varepsilon_0(1+\varepsilon_r)}{\pi}\cosh^{-1}\left(\frac{W+g}{g}\right) \tag{3}$$

where μ_o is the free space permeability, and ϵ_o is the free space permittivity. From the LC model shown in Figure 10(b), the surface impedance of mushroom-like EBG structure is given by

$$f_r = \frac{1}{2\pi\sqrt{L_1(C_1+C_0)}} \tag{4}$$

Band gap can be tuned to any interfering frequency using optimization of the parameters like inductor L that results from thin connecting lines of EBG cell, and capacitance C results from gaps within the cell. The band gap is defined as a frequency band where no mode is propagated. Similarly, the frequency band gap can be calculated using the following formulae [35].

$$\omega_r = \frac{1}{\sqrt{LC}} \tag{5}$$

$$BW = \frac{\Delta\omega}{\omega_r} = \frac{1}{\eta_0}\sqrt{\frac{L}{C}} \tag{6}$$

where η is the impedance of the free space of the value 120π.

The impedance is inductive and supports TM surface waves at low frequencies. At high frequencies, it becomes capacitive and supports TE surface waves. A frequency band gap occurs because the EBG does not support surface waves, and high impedance is attained close to the resonance frequency ω_r. In addition, the high surface impedance prevents the phase reversal that occurs on a perfect electric conductor (PEC) when a plane wave is reflected.

The EBG geometry determines the values of the inductance L and capacitance C, and its resonance behaviour is used to explain the band gap feature of the EBG structure. These insights are relatively straightforward, but their interpretations are not highly accurate due to the simplified approximation of L and C. The periodic transmission line method and full wave numerical methods, which are complex in nature, can be used to analyse various EBG characteristics such as surface impedance, reflection phase, dispersion curve, and band gaps [34–38].

As the frequency increases, the reflection phase characteristics shift from $+180°$ to $-180°$. This structure exhibits similar reflection phase characteristics to the PEC surface at lower and higher frequency regions. The EBG structure has zero degree of reflection phase at the frequency of resonance, and this repeats at multiple bands across the extreme wide band spectrum, such that no surface waves can propagate in the EBG structure within this frequency band gap, as illustrated in Figure 12.

The 3D gain polar plot and radiation patterns produced by the proposed antenna simulation at resonance frequencies of 27 GHz, 59 GHz, 75 GHz, 241 GHz, 305 GHz, 387 GHz, 511 GHz, 551 GHz, and 617 GHz are shown in Figure 13. At resonant frequencies, the corresponding maximum peak gains are 6.74 dB, 9.72 dB, 9.83 dB, 13.54 dB, 14.84 dB, 16.24 dB, 17.91 dB, 16.75 dB, and 16.83 dB. At

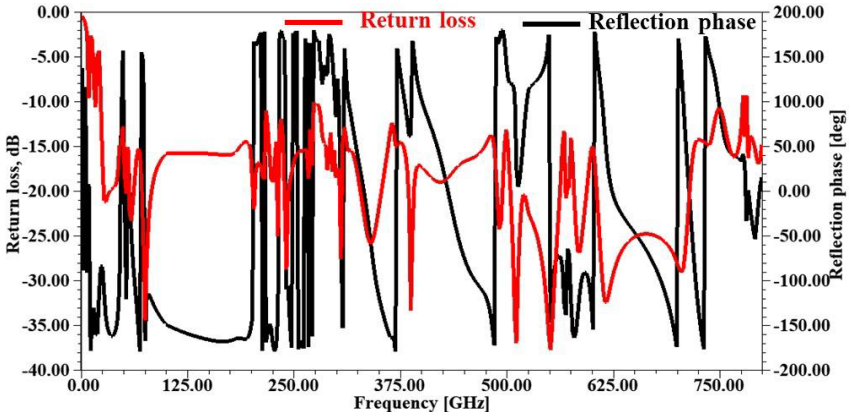

Figure 12. Variation of reflection phase with frequency of proposed EWB antenna.

all resonance frequencies, two-dimensional simulated radiation patterns in the elevation and azimuthal planes (E-plane and H-plane) are characterised in Figure 13. Co- and cross-polarization representations at resonance frequencies of 27 GHz, 59 GHz, 75 GHz, 241 GHz, 305 GHz, 387 GHz, 511 GHz, 551 GHz, and 617 GHz are demonstrated in Figures 13(a)–(i). From Figures 13(a)–(i), it is observed that an omnidirectional pattern is produced for both co- and cross-polarization patterns. Figures 10(a)–(i) depict simulated gain polar plots and radiation patterns for each resonance frequency, demonstrating outstanding performance and supporting high-frequency wireless applications.

Figures 14(a)–(i) show that at resonant frequencies, the surface current distribution is perceived more strongly at the feed line. At low frequencies, the magnitude of the current is centred at the proposed patch structure, and the impedance at the feed line and patch region is precisely matched. At resonant frequencies of 27 GHz, 59 GHz, 75 GHz, 241 GHz, 305 GHz, 387 GHz, 511 GHz, 551 GHz, and

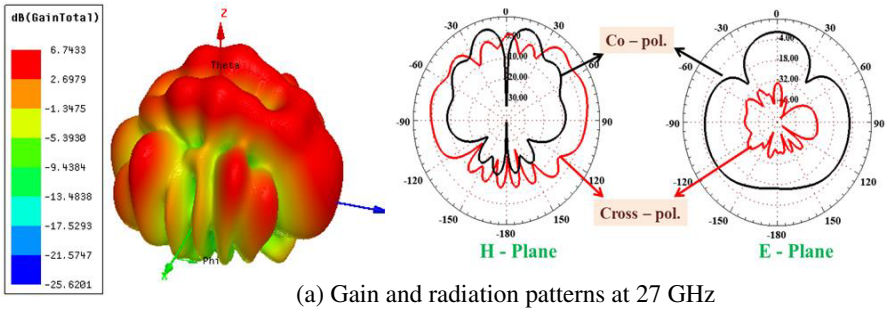

(a) Gain and radiation patterns at 27 GHz

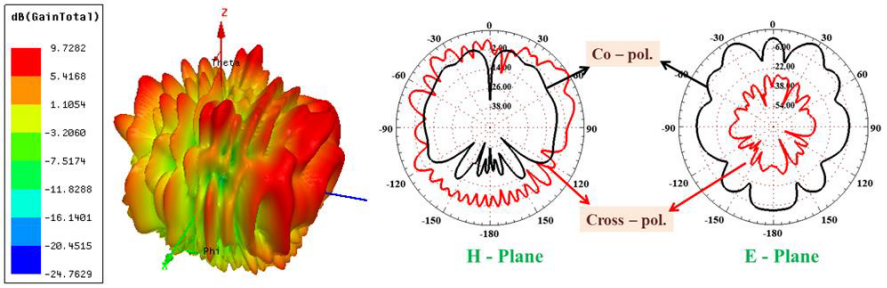

(b) Gain and radiation patterns at 59 GHz

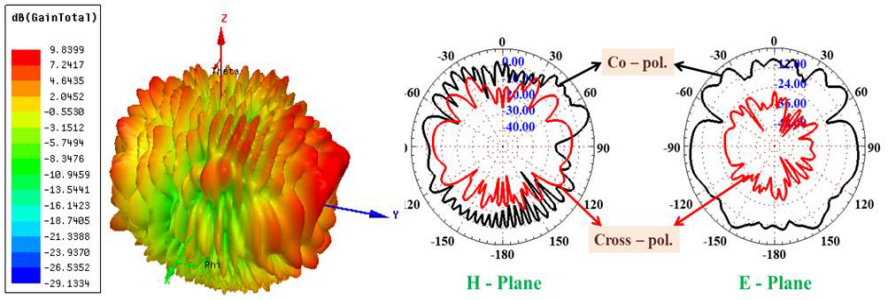

(c) Gain and radiation patterns at 75 GHz

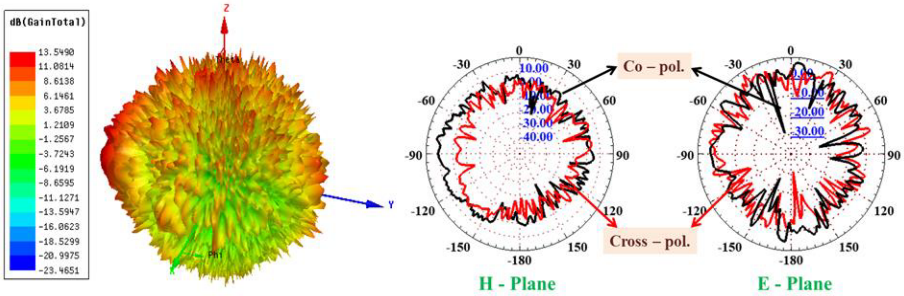

(d) Gain and radiation patterns at 241 GHz

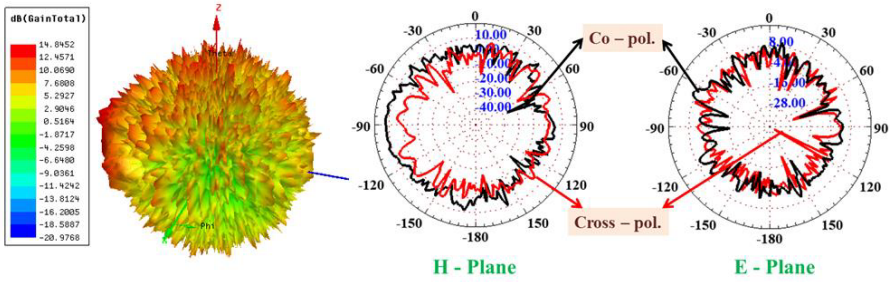

(e) Gain and radiation patterns at 305 GHz

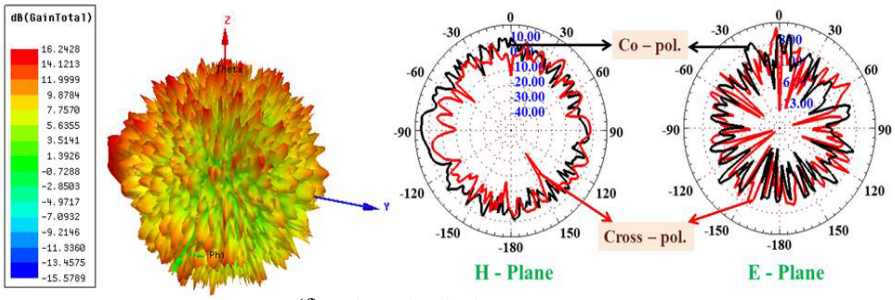

(f) Gain and radiation patterns at 387 GHz

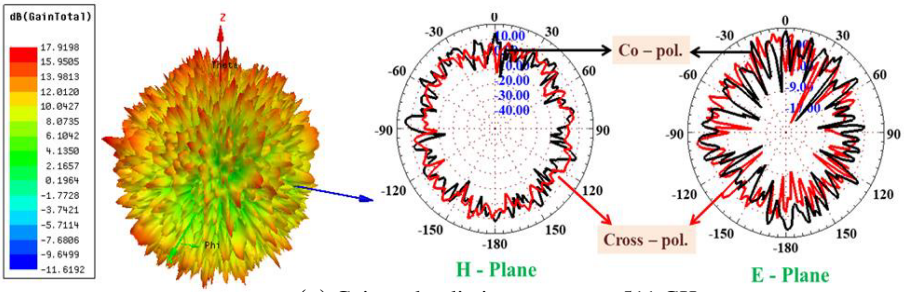

(g) Gain and radiation patterns at 511 GHz

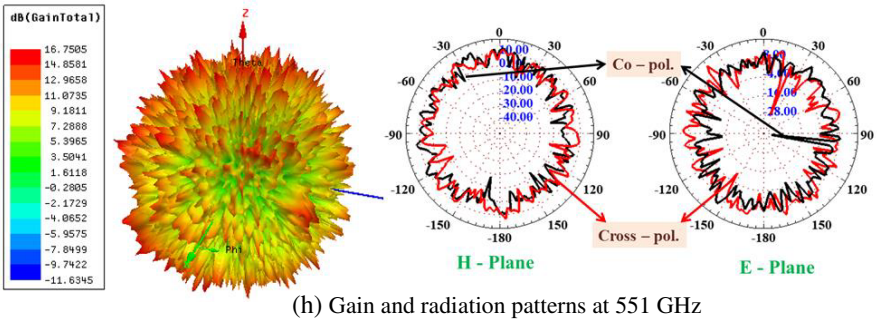

(h) Gain and radiation patterns at 551 GHz

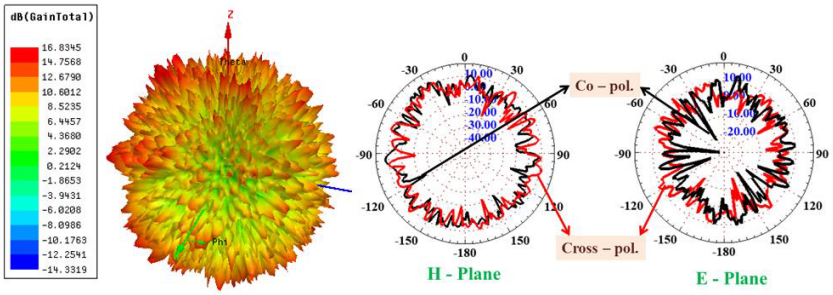

(i) Gain and radiation patterns at 617 GHz

Figure 13. Far-field reports of proposed antenna at (a) 27 GHz, (b) 59 GHz, (c) 75 GHz, (d) 241 GHz, (e) 305 GHz, (f) 387 GHz, (g) 511 GHz, (h) 551 GHz, (i) 617 GHz.

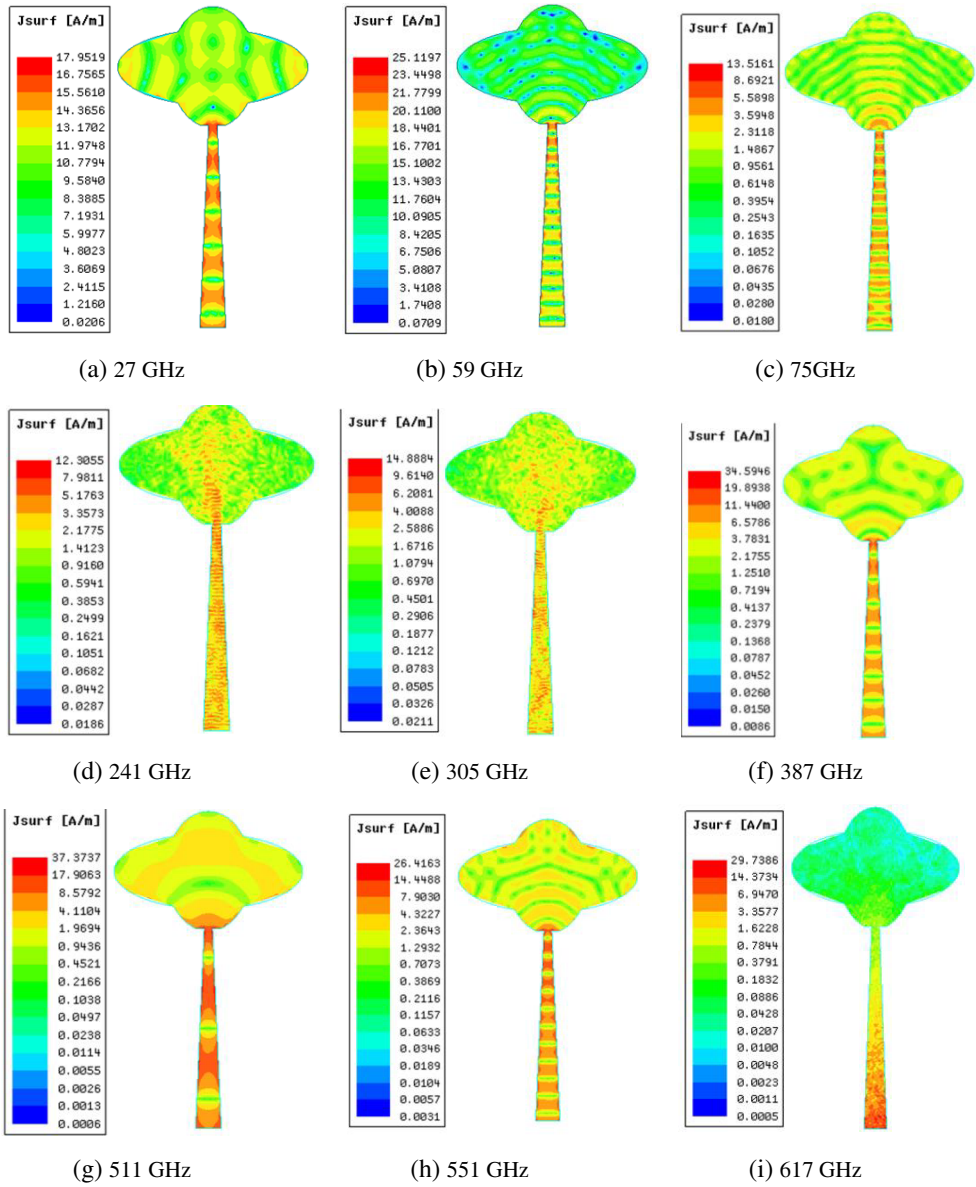

(a) 27 GHz (b) 59 GHz (c) 75GHz

(d) 241 GHz (e) 305 GHz (f) 387 GHz

(g) 511 GHz (h) 551 GHz (i) 617 GHz

Figure 14. Surface current distribution of proposed antenna at various frequencies.

617 GHz, the antenna impedance is based on the features of the redesigned structure, tapered feed, and EBG slots in the dielectric material.

The simulated gain characteristics of the suggested antenna in response to frequency are shown in Figure 15. The antenna gain value increases with frequency, but there are some frequency-dependent declines due to the modified structure and the integration of EBG slots in the substrate material. The maximum peak gain obtained at a resonant frequency of 511 GHz is 17.91 dB. The radiation efficiency (η) of the proposed antenna is demonstrated in Figure 16. The designed antenna has high radiation efficiency at low frequencies. As shown in Figure 16, at high frequencies, the radiation efficiency gradually decreases as the design modifies the current density. This causes a delay in the path of EM waves within the antenna, which reduces the radiation efficiency.

Table 3 shows the computed antenna parameters of the proposed antenna at resonance frequencies of 27 GHz, 59 GHz, 75 GHz, 241 GHz, 305 GHz, 387 GHz, 511 GHz, 551 GHz, and 617 GHz, such as maximum radiation intensity (U), incident power, accepted power, radiated power, peak gain, peak realised gain, peak directivity, front-to-back ratio (FBR) radiation, and efficiency.

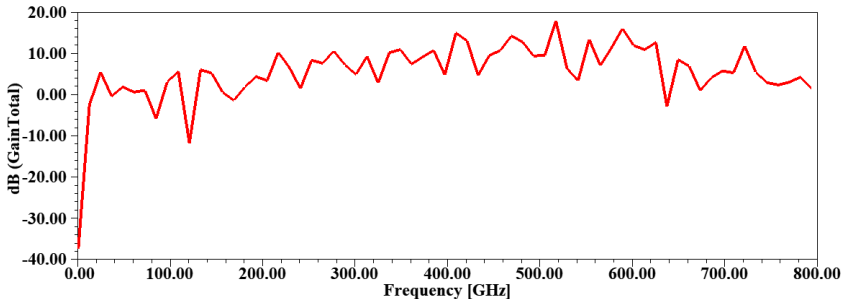

Figure 15. Gain characteristics of a tapered-fed modified monopole antenna with an EBG structure.

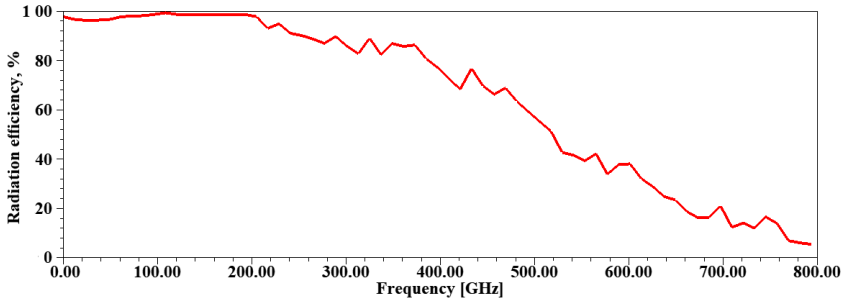

Figure 16. Radiation efficiency characteristics of a tapered-fed modified monopole antenna with an EBG structure.

Table 3. Computed antenna parameters of the proposed antenna at resonance frequencies.

S. No	Parameters	27 GHz	59 GHz	75 GHz	241 GHz	305 GHz	387 GHz	511 GHz	551 GHz	617 GHz
1	Max U (mW/Sr)	3.65	7.45	7.56	17.59	23.85	33.38	48.66	37.64	36.70
2	Peak directivity (dB)	4.86	9.65	9.82	24.83	35.53	52.20	120.45	120.35	150.35
3	Peak gain (dB)	4.72	9.39	9.63	22.61	30.56	42.09	61.94	47.32	48.24
4	Peak realized gain (dB)	4.58	9.36	9.51	22.16	29.97	41.95	61.15	47.31	46.12
5	Radiated power (mW)	9.42	9.70	9.67	8.89	8.42	8.03	5.07	3.93	3.06
6	Accepted power (mW)	9.70	9.96	9.86	9.76	9.82	9.96	9.87	9.99	9.55
7	Incident power (mW)	10	10	10	10	10	10	10	10	10
8	Radiation efficiency (%)	97.12	97.34	98.07	91.02	85.73	80.64	51.42	39.31	32.08
9	Front to back ratio	24.19	26.09	6.68	36.85	16.54	14.68	8.45	14.46	6.08

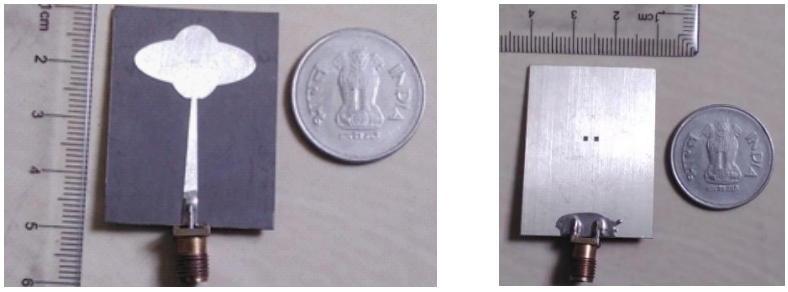

(a) Front view (b) Rear view

Figure 17. Fabricated designed antenna.

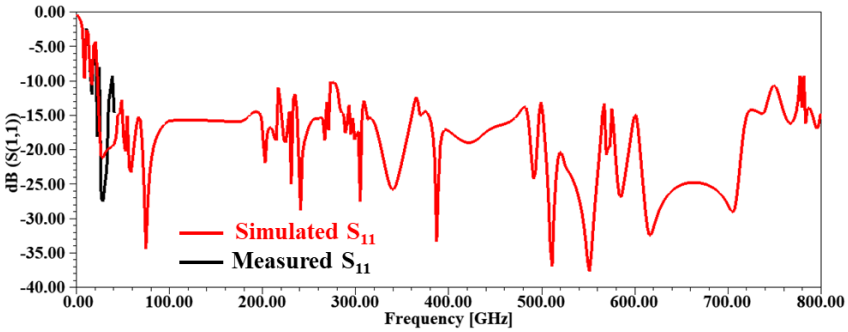

Figure 18. Simulated and measured return loss characteristics of the designed ellipsoid antenna.

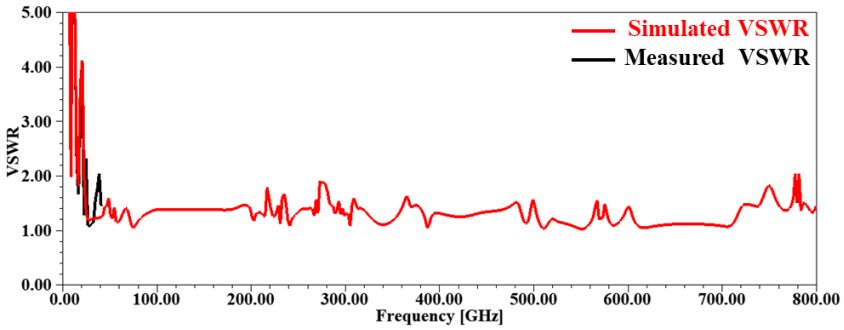

Figure 19. Simulated and measured VSWR characteristics of the designed ellipsoid antenna.

Figure 17 shows the front and back views of the fabricated proposed SWB antenna. The fabricated chip is connected to the VNA cable through an SMA (Sub Miniature Version A) connector. The performance comparisons of simulated and measured results of return loss (S_{11}) and VSWR characteristics of the proposed antenna model are shown in Figures 18 and 19. It can be observed that simulated and measured results are in good agreement, but there is a discrepancy in the characteristics at 46 GHz due to the soldering and etching processes. Out of this, S_{11} characteristics are lower than -10 dB, and VSWR is less than 2. The range of the VNA analyzer is 40 GHz, so the parameters of the model are measured up to that frequency.

The proposed EBG structures can be used as an efficient alternative to traditional ground planes in low-profile antennas to achieve extreme bandwidth and efficiency, as the radiation efficiency of a low-profile wire antenna is very low when a perfect electrical conductor (PEC) is used as the ground plane. This is due to interference in the far field between the radiating field and the field generated by the ground plane's image current. Alternately, the ground can be thought of as an ideal conductor,

Table 4. Comparison of proposed EWB antenna other proposed structures and other reported works.

Ref.	Size (mm^2)	Substrate	h, mm	BW, GHz	IBW ($f_h - f_l$)	BR (f_h/f_l)	FBW $2*(f_h-f_l)/(f_h+f_l)*100$	Peak G, dB	Peak η%
1	24 × 18	RT Duroid	0.787	50–200	150	4	1.2	13.9	NA
2	90 × 56	FR4	1.6	3.34–4.8 5.5–10.6 13–14.96	1.54 5.1 1.96	1.43 1.92 1.15	0.38 0.63 0.14	5	NA
3	52.25 × 42	Rogers RT/Duroid 5870	1.575	1.30–20	18.7	15.38	1.75	4.18	NA
4	11 × 15	FR4	1	5–15	10	3	1	4.9	NA
5	25 × 26	FR4	1.6	2.43–32.93	30.5	13.55	1.72	7.35	NA
6	40 × 40	NA	66	3–18	15	6	1.42	3.2	98.9
7	30 × 28	FR4 epoxy	1.6	3.4–37.4	34	11	1.66	11	98
8	30 × 10	FR4	1.6	3.1–10.6	7.5	2.94	1.09	15	>70
9	30 × 45	AgHT-8	0.175	3.15–32	28.85	10.15	1.64	–4.8	NA
10	14 × 22	FR4	1.6	3.9–18	14.1	4.6	1.28	NA	NA
11	38 × 55	FR4	1.6	3–35 GHz	32	11.66	1.68	6d	NA
12	20 × 28	LCP	0.225	2.85–11.85	9	4.15	1.22	3.2	NA
13	22 ×18.5	FR4-epoxy	1.6	3.5–37.2	33.7	10.6	1.65	13.7	98
14	50 × 40	Rogers RO4003C	0.508	3.5–10.6	7.1	3.02	1.007	4.7	73
15	32 × 22	FR4	1.60	2.5–29	26.5	11.6	1.68	6.10	75
16	35 × 30	FR4	1.52	3.9–14	10.1	3.58	1.12	11	NA
17	36 × 150	NA	0.5	0.4–16	15.6	40	1.9	10.5	NA
18	30 × 30	F4B	1.6	2.11–5.01	2.9	2.37	0.81	5.14	58.7
19	110 × 124	NA	1.524	1.02–24.1	23.08	23.62	1.844	7.1	76
20	25 × 20	FR4	1.6	2.51–16.48	13.97	6.565	1.47	5.25	NA
21	120 × 124	Rogers4350B	1.5	1.08–27.4	26.32	25.37	1.84	3.8	NA
22	60 × 50	FR4	1.59	2.05–3.05 3.65–3.92 5.24–10.75	1 0.27 5.51	1.48 1.03 2.05	0.39 0.07 0.68	8.03	NA
23	47.85 × 35	Rogers 4003C	1.524	2.38–13.74	11.36	5.7	1.40	4.41	NA
24	140 × 100	FR4	1	0.4–20	19.6	50	1.92	6.3	96
25	12 × 4.6	Rogers RT/Duroid	0.8	24–40	16	1.666	0.5	5.77	84
26	20 × 15	FR4	1.6	4.9–25	20.1	5.10	1.34	4	NA
27	20 × 20	Rogers RT5880	0.787	17.22–180	162.78	10.45	1.65	10	NA
28	52.25 × 42	Rogers RT/duroid 5880	1.575	0.96–10.9	9.94	11.35	1.67	3.5	NA
29	19 × 31	FR4-epoxy	1.6	3–60	57	20	1.80	11.9	NA
30	30 × 28	Rogers R04003	0.5	3.30–3.60 5.15–5.350 5.725–5.825 7.0–7.40 8.10–8.50	0.30 0.20 0.1 0.40 0.40	1.09 1.03 1.01 1.05 1.04	0.086 0.038 0.017 0.055 0.048	4	98
This work	**30 × 40**	**Rogers RT/ Duroid 5880**	**0.787**	**23.16 –776.59**	**753.43**	**33.53**	**188.41**	**17.91**	**99.4**

which is useful as a reflector but causes the phase reversal of the reflected wave due to its negative reflection coefficient. Additionally, ideal conductors promote the propagation of TM surface waves, which degrades antenna performance.

3. PERFORMANCE COMPARISON OF PROPOSED WORK WITH EARLIER REPORTED WORKS

Table 4 summarises the benefits of the proposed antenna design in comparison to several existing antennas [1–30] presented in this section. The proposed antenna is described by its overall size, the material used for the substrate, height (h) of the dielectric material, operating bandwidth (BW) range, impedance bandwidth (IBW), fractional impedance bandwidth (FBW), bandwidth ratio (BR), peak gain (G), and peak radiation efficiency (η). The proposed antenna has an extremely broad frequency range spanning from 23.1 to 776.5 GHz. It has a maximum FBW of 188.41. The suggested antenna has a maximum gain of 17.91 dB and radiation efficiency of 99.4%. According to Table 4, the proposed antenna is appropriate for wireless technology such as radar systems, cellular, satellite, and medical imaging.

4. CONCLUSION

A modified elliptical monopole antenna fed with a tapered transmission line using the EBG technique is employed for extreme wide band (EWB) applications, which improves impedance bandwidth and gain. This proposed antenna is simulated using an HFSS solver and fabricated on Rogers RT/Duroid 5880 dielectric substrate material with a relative permittivity of 2.2 and a loss tangent of 0.0009. The proposed monopole antenna achieves an FBW of 188.41%, which is the highest FBW among the existing models [1–30]. It also offers simulated frequency range from 23.16 GHz to 776.59 GHz and a bandwidth ratio of 33.53. Input impedance at resonance frequencies of the proposed antenna indicates that the designed antenna has negligible impedance mismatch losses. Simulated peak gain is 17.91 dB, and its radiation efficiency is 99.4%. The omnidirectional radiation mechanism is obtained in both co- and cross-polarized radiation patterns, and it maintains 90% of stable radiation characteristics. It is proven that the proposed antenna performs better than the existing models. Because of these benefits, the proposed antenna is used in millimetre wave spectrum applications such as Ka-band (26.5–40 GHz), V-band (40–75 GHz), W-band (75–110 GHz), millimetre band (110–300 GHz), and low frequency terahertz (THz).

Author Contribution

Both the authors contributed to the study, conception, design, and simulations. Data collection, analysis, and simulation were performed by N. Suguna and S. Revathi. Both authors have read and agreed to the published version of the manuscript.

Data Availability

All the data generated during and/or analysed during the current study are available from the corresponding author on reasonable request.

Conflict of Interest

The authors declare that there is no conflict of interest.

ACKNOWLEDGMENT

This work is not supported by the any funding agency.

The authors would like to thank the reviewers for their careful and in-depth evaluation of the manuscript.

REFERENCES

1. Bernety, H. M., B. Zakeri, and R. Gholami, "A compact directional super-wideband antenna," *2013 21st Iranian Conference on Electrical Engineering (ICEE)*, 1–4, 2013, doi:10.1109/iraniancee.2013.65996.
2. Pandey, S. K., G. P. Pandey, and P. M. Sarun, "Fractal based triple band high gain monopole antenna," *Frequenz*, Vol. 71, Nos. 11–12, 2017, doi:10.1515/freq-2016-0208.
3. Samsuzzaman, M. and M. T. Islam, "A semicircular shaped super wideband patch antenna with high bandwidth dimension ratio," *Microwave and Optical Technology Letters*, Vol. 57, No. 2, 445–452, 2014, doi:10.1002/mop.28872.
4. Ellis, M. S., Z. Zhao, J. Wu, Z. Nie, and Q. H. Liu, "Small planar monopole ultra-wideband antenna with reduced ground plane effect," *IET Microw Antennas Propag.*, Vol. 9, No. 10, 1028–1034, 2015.
5. Aziz, S. Z. and M. F. Jamlos, "Compact super wideband patch antenna design using diversities of reactive loaded technique," *Microwave and Optical Technology Letters*, Vol. 58, No. 12, 2811–2814, 2016, doi:10.1002/mop.30152.
6. Nadeem, M., A. N. Khan, A. Ali Khan, and T. Azim, "Low profile CPW fed slotted planar inverted cone ultra-wide band antenna for WBAN applications," *Microwave and Optical Technology Letters*, Vol. 60, No. 4, 870–876, 2018, doi:10.1002/mop.31070.
7. Singhal, S. and A. K. Singh, "CPW-fed hexagonal Sierpinski super wideband fractal antenna," *IET Microwaves, Antennas & Propagation*, Vol. 10, No. 15, 1701–1707, 2016, doi:10.1049/iet-map.2016.0154.
8. Addaci, R. and T. Fortaki, "Miniature low profile UWB antenna: New techniques for bandwidth enhancement and radiation pattern stability," *Microwave and Optical Technology Letters*, Vol. 58, No. 8, 1808–1813, 2016, doi:10.1002/mop.29907.
9. Hakimi, S., S. K. A. Rahim, M. Abedian, S. M. Noghabaei, and M. Khalily, "CPW-fed transparent antenna for extended ultrawideband applications," *IEEE Antennas and Wireless Propagation Letters*, Vol. 13, 1251–1254, 2014, doi:10.1109/lawp.2014.2333091.
10. Hendevari, M. S., A. Pourziad, and S. Nikmehr, "A novel ultra-wideband monopole antenna for ground penetrating radar application," *Microwave and Optical Technology Letters*, Vol. 60, No. 9, 2252–2256, 2018, doi:10.1002/mop.31335.
11. Gorai, A., A. Karmakar, M. Pal, and R. Ghatak, "A CPW-fed propeller shaped monopole antenna with super wideband characteristics," *Progress In Electromagnetics Research C*, Vol. 45, 125–135, 2013.
12. Nikolaou, S. and M. A. B. Abbasi, "Design and development of a compact UWB monopole antenna with easily-controllable return loss," *IEEE Transactions on Antennas and Propagation*, Vol. 65, No. 4, 2063–2067, 2017, doi:10.1109/tap.2017.2670322.
13. Singhal, S. and A. K. Singh, "CPW-fed Phi-shaped monopole antenna for super-wideband applications," *Progress In Electromagnetics Research C*, Vol. 64, 105–116, 2016.
14. Omar, A. A., O. Abu Safia, and M. Nedil, "UWB coplanar waveguide-fed coplanar strips rectangular spiral antenna," *International Journal of RF and Microwave Computer-Aided Engineering*, Vol. 27, No. 7, e21115, 2017, doi:10.1002/mmce.21115.
15. Rahman, M. N., M. T. Islam, M. Z. Mahmud, and M. Samsuzzaman, "Compact microstrip patch antenna proclaiming super wideband characteristics," *Microwave and Optical Technology Letters*, Vol. 59, No. 10, 2563–2570, 2017, doi:10.1002/mop.30770.
16. Hayouni, M., F. Choubani, T. H. Vuong, and J. David, "Main effects ensured by symmetric circular slots etched on the radiating patch of a compact monopole antenna on the impedance bandwidth and radiation patterns," *Wireless Pers. Commun.*, Vol. 95, No. 4, 4243–4256, 2017.
17. Dong, Y., W. Hong, L. Liu, Y. Zhang, and Z. Kuai, "Performance analysis of a printed super-wideband antenna," *Microwave and Optical Technology Letters*, Vol. 51, No. 4, 949–956, 2009, doi:10.1002/mop.24222.
18. Wu, B. J. and Q. Y. Feng, "A novel compact broadband antenna for LTE/WLAN/WiMAX applications," *Progress In Electromagnetics Research Letters*, Vol. 59, 129–135, 2016.

19. Liu, J., S. Zhong, and K. P. Esselle, "A printed elliptical monopole antenna with modified feeding structure for bandwidth enhancement," *IEEE Transactions on Antennas and Propagation*, Vol. 59, No. 2, 667–670, 2011, doi:10.1109/tap.2010.2096398.
20. Tiwari, R. N., P. Singh, and B. K. Kanaujia, "Small-size scarecrow-shaped CPW and microstrip-line-fed UWB antennas," *Journal of Computational Electronics*, Vol. 17, No. 3, 1047–1055, 2018, doi:10.1007/s10825-018-1182-0.
21. Liu, J., K. P. Esselle, S. G. Hay, and S. Zhong, "Achieving ratio bandwidth of 25 : 1 from a printed antenna using a tapered semi-ring feed," *IEEE Antennas and Wireless Propagation Letters*, Vol. 10, 1333–1336, 2011, doi:10.1109/lawp.2011.2177800.
22. Srivastava, K., A. Kumar, B. K. Kanaujia, S. Dwari, and S. Kumar, "Multiband integrated wideband antenna for bluetooth/WLAN applications," *AEU — International Journal of Electronics and Communications*, Vol. 89, 77–84, 2018, doi: 10.1016/j.aeue.2018.03.027.
23. Bozdag, G. and A. Kustepeli, "Wideband planar monopole antennas for GPS/WLAN/WiMAX/UWB and X-band applications," *Microwave and Optical Technology Letters*, Vol. 58, No. 2, 257–261, 2015, doi:10.1002/mop.29550.
24. Yang, L., D. Zhang, X. Zhu, and Y. Li, "Design of a super wide band antenna and measure of ambient RF density in urban area," *IEEE Access*, Vol. 8, 767–774, 2020, doi:10.1109/access.2019.2962141.
25. Ramanuajam, P., C. Arumugam, R. Venkatesan, and M. Ponusamy, "Design of compact patch antenna with enhanced gain and bandwidth for 5G mm-wave applications," *IET Microwaves, Antennas & Propagation*, Vol. 14, No. 12, 1455–1461, 2020, doi:10.1049/iet-map.2019.0891.
26. Elhabchi, M., M. N. Srifi, and R. Touahni, "A novel CPW-fed semi-circular triangular antenna with modified ground plane for super ultra-wide band (UWB) applications," *2018 International Symposium on Advanced Electrical and Communication Technologies (ISAECT)*, 1–5, 2018, doi:10.1109/isaect.2018.8618857.
27. Malik, R., P. Singh, H. Ali, and T. Goel, "A star shaped superwide band fractal antenna for 5G applications," *2018 3rd International Conference for Convergence in Technology (I2CT)*, 1–6, 2018, doi:10.1109/i2ct.2018.8529404.
28. Okas, P., A. Sharma, G. Das, and R. K. Gangwar, "Elliptical slot loaded partially segmented circular monopole antenna for super wideband application," *AEU — International Journal of Electronics and Communications*, Vol. 88, 63–69, 2018, doi: 10.1016/j.aeue.2018.03.004.
29. Srikar, D. and S. Anuradha, "A compact super wideband antenna for wireless communications," *2018 9th International Conference on Computing, Communication and Networking Technologies (ICCCNT)*, 1–4, 2018, doi:10.1109/icccnt.2018.8494146.
30. Rahman, M., W. T. Khan, and M. Imran, "Penta-notched UWB antenna with sharp frequency edge selectivity using combination of SRR, CSRR, and DGS," *AEU — International Journal of Electronics and Communications*, Vol. 93, 116–122, 2018, doi: 10.1016/j.aeue.2018.06.010.
31. Mythili, P. and A. Das, "Simple approach to determine resonant frequencies of microstrip antennas," *IEE Proceedings — Microwaves, Antennas and Propagation*, Vol. 145, No. 2, 159–162, 1998.
32. Ray, K. P. and G. Kumar, "Determination of the resonant frequency of microstrip antennas," *Microwave and Optical Technology Letters*, Vol. 23, No. 2, 114–117, 1999.
33. Sievenpiper, D., "High-impedance electromagnetic surfaces," Ph.D. Dissertation, UCLA, 1999, Available at www.ee.ucla.edu/labs/photon/thesis/ThesisDan.pdf.
34. Yang, F. and Y. Rahmat-Samii, "Reflection phase characterizations of the EBG ground plane for low profile wire antenna applications," *IEEE Transactions on Antennas and Propagation*, Vol. 51, No. 10, 2691–2703, 2003, doi: 10.1109/TAP.2003.817559.
35. Shaban, H. F., H. A. Elmikaty, and A. A. Shaalan, "Study the effects of electromagnetic band-gap (EBG) substrate on two patch microstrip antenna," *Progress In Electromagnetics Research B*, Vol. 10, 55–74, 2008.
36. Elsheakh, D. M., H. A. Elsadek, and E. A. Abdallah, "Antenna designs with electromagnetic band gap structures," *Metamaterial*, InTech, Rijeka, Croatia, 403–473, 2012.

37. Yang, F. and Y. Rahmat Samii, "Reflection phase characterizations of the EBG ground plane for low profile wire antenna," *IEEE Transactions on Antennas and Propagation*, Vol. 51, No. 10, 2691–2703, Oct. 2003.
38. Elsheakh, D. N., H. A. Elsadek, E. A. Abdallah, H. Elhenawy, and M. F. Iskander, "Enhancement of microstrip monopole antenna bandwidth by using EBG structures," *IEEE Antennas and Wireless Propagation Letters*, Vol. 8, 959–962, 2009, doi: 10.1109/LAWP.2009.2030375.